Supercell Design for First-Principles Simulations of Solids and Application to Diamond, Silica, and Superionic Water

B. Militzer[a]

[a]*Department of Earth and Planetary Science, Department of Astronomy, University of California, Berkeley, CA 94720, USA*

Abstract

For efficient first-principles computation of crystalline materials at high density and temperature, an optimal choice of the supercell is important to minimize finite size errors. An algorithm is presented to construct compact supercells for arbitrary crystal structures. Rather than constructing standard supercells by replicating the conventional unit cell, we employ the full flexibility that we gain by using arbitrary combinations of the primitive cell vectors in order to construct a series of cubic and nearly cubic supercells. In cases where different polymorphs of a material needed to be compared, we are able construct supercells of consistent size. Our approach also allows us to efficiently study the finite size effects in systems like superionic water where they would otherwise difficult to obtain because a standard replication of the unit cells leads to supercells that are too expensive to be used for first-principles simulations. We apply our method to simple, body-centered, and face-centered cubic as well as hexagonal close packed cells. We present simulation results for diamond, silica in the pyrite structure, and superionic water with an face-centered cubic oxygen sub-lattice. The effects of the finite simulation cell size and Brillouin zone sampling on the computed pressure and internal energy are analyzed.

Keywords: Ab initio molecular dynamics, density functional theory

1. Introduction

First-principles computer simulations contribute to our understanding of a wide range of phenomena in physics [1], chemistry [2], geophysics [3, 4, 5], and to some extend also in molecular biology [6]. While ground-state calculations of crystalline materials can often be performed in primitive crystallographic cells with a small number of atoms, simulations at finite temperature require cells with a much larger number of atoms. To simulate liquids, one typically chooses cubic cells [7] and increases the number of atoms until the artificial correlation, that is introduced by the periodic boundary conditions, has a negligible impact on the computed properties [8]. Simulations of crystalline materials often require the consideration of a comparable number of atoms. Therefore, one

Email address: militzer@berkeley.edu (B. Militzer)
URL: http://militzer.berkeley.edu (B. Militzer)

constructs supercells by replicating the primitive cell in all spatial directions. Such supercells allow one to perform density functional molecular dynamics simulations (DFT-MD) to determine the thermodynamic properties of solids [9, 10, 11] at elevated temperatures where the quasi-harmonic approximation is no longer applicable [12]. Quasi-harmonic calculations typically use primitive cells and perturbation theory [13] but, occasionally, supercells are still in use [14]. Supercells are also employed to study the effects of disorder in different types of alloys and solid solutions [15, 16, 17, 18]. Computational studies of defects in solids also require supercells to reduce the interaction between defect images [19, 20, 21, 22, 23, 24, 25, 26, 27]. For simulations of materials with incommensurate crystal structures, one also constructs periodic supercells that approximate incommensurate spatial periodicities as close as possible [28, 29]. The determination of the magnetic state of a structure with multiple transition metal atoms may also require supercells [30, 31, 32]. The computation of x-ray absorption near edge structures (XANES) is performed in supercells [33]. Direct melting simulations and the two-phase methods [34, 35] also rely on supercells. Variable cell dynamics simulations [3] as well as the study of amorphization [36] and other structural changes in solids [37] employ supercells as well. Quantum Monte Carlo (QMC) calculations employ supercells to better capture the interaction effect between all electrons [38, 4, 39]. Since QMC calculations are significantly more expensive than density functional simulations, one is even more constrained when choosing the supercell.

Despite all these applications, no general algorithm exists to construct appropriate supercells molecular dynamics or Monte Carlo simulation where one wants to minimize the artificial interaction between period images. For cubic cells, one typically replicates the unit cell uniformly in all spatial directions, $n \times n \times n$. This may, however, lead rather rapidly to cells that are prohibitively expensive. In the case of superionic water in a face-centered cubic (fcc) structure, the cubic unit cell has four water molecules. Thus, in Ref. [40], most simulations were performed in a $2 \times 2 \times 2$ with supercell with 32 molecules and only one, rather demanding finite-size test with 108 molecules was conducted. In an earlier study of body-centered cubic (bcc) superionic water [41], results for $2 \times 2 \times 2$ and $3 \times 3 \times 3$ supercells with 56 and 128 molecules, respectively, were reported. No other cells were considered while, as we demonstrate in the article, a number of intermediate nearly cubic cells could have been chosen to facilitate a more efficient finite-size analysis.

Supercells of different shapes have constructed to study solid solutions where, e.g., atoms of type A or B can occupy the sites in an fcc or bcc lattice [42]. Algorithms have been advanced to generate *all possible* configurations for a given supercell size [43] and efficient methods exit to remove symmetry-equivalent configurations [44]. The goal of our algorithm is different, however. We do not deal with atomic disorder and, rather than generating all possible supercells, we want to construct the best possible supercell for a given size in order to minimize finite-size effects in many-body simulations.

The question of choosing the appropriate supercell becomes even more difficult when one deals with non-cubic primitive cells. For orthorhombic structures, one may construct $n_1 \times n_2 \times n_3$ supercells that are nearly cubic while preserving the orthorhombic character. For arbitrary triclinic cells, it is less obvious how to proceed. For water ice at megabar pressures [45], a monoclinic structure with $P2_1$ symmetry, an orthorhombic structure with $Pcca$, and a hexagonal structure with $P3_121$ symmetry have recently been predicted to form at zero temperature [46]. To determine whether these groundstate structures lead to superionic systems that are thermodynamically more stable than the recently

predicted fcc structure, one needs to construct supercells, heat the structure up in with DFT-MD simulations and compare their Gibbs free energies that may be obtained via thermodynamic integration (TDI) [40]. For the monoclinic, orthorhombic, hexagonal structures, one would want to construct supercells that are again nearly cubic. Ideally one would choose a cell of comparable size as in the bcc and fcc calculations but there is no straightforward method available to construct such cells.

The question how to construct supercells of comparable size for different structures will always be relevant when a material has different polymorphs that need to be compared. Silica, SiO_2 is a archetypal example with more than ten crystal structures [4, 5]. Its pyrite-type polymorph has a cubic unit cell with 12 atoms. We will demonstrate that various reasonable supercell choices exist in additiona to a simple $n \times n \times n$ replication.

Recently, significant progress has been made in predicting groundstate crystal structures with evolutionary algorithms [47], random search techniques [48, 46], and others methods [49], and number of theoretical predictions have later been confirmed experimentally [50]. Crystal structure prediction at higher temperature outside of the quasi-harmonic regime is more difficult and requires the comparison of the Gibbs free energy of thousands of structures. Supercells need to be constructed in order to facilitate DFT-MD simulations and TDI calculations [51, 52, 53, 54, 55]. Rather than relying on human intervention, we would want to use a computer algorithm that constructs reasonable supercells automatically for any cell shape, which is the goal of this article.

2. Methods

Rather than constructing standard $n \times n \times n$ supercells by replicating the conventional unit cell, we employ the full flexibility that we gain by using an arbitrary combination of the primitive cell vectors, $\vec{a}$, $\vec{b}$, and $\vec{c}$. We construct vectors of the supercell from a linear combination of the primitive cell vectors [56],

$$\begin{aligned} \vec{a}_{\rm SS} &= i_a\vec{a} + j_a\vec{b} + k_a\vec{c} \ , \\ \vec{b}_{\rm SS} &= i_b\vec{a} + j_b\vec{b} + k_b\vec{c} \ , \\ \vec{c}_{\rm SS} &= i_c\vec{a} + j_c\vec{b} + k_c\vec{c} \ . \end{aligned} \tag{1}$$

For each supercell vector, the coefficients i, j, and k are arbitrary integers that we restrict to take values from $-n$ to n. We typically set n between 5 and 10. j_a, k_a, and k_b can be set zero for bcc and fcc lattices [44]. In general, however, the construction of a supercell turns into a 9-dimensional optimization problem but symmetry arguments can be used to reduce the search space significantly,

$$\begin{aligned} \left[\vec{a}_{\rm SS}, \vec{b}_{\rm SS}, \vec{c}_{\rm SS}\right](V_{\rm SS}) \quad = \quad & \max_{i_a=1}^{n} \ \max_{j_a=-n}^{n} \ \max_{\substack{k_a=-n \\ |\vec{a}_{\rm SS}|>0}}^{n} \ \max_{i_b=-i_a}^{i_a} \ \max_{j_b=-n}^{n} \ \max_{\substack{k_b=-n \\ |\vec{b}_{\rm SS}|>0}}^{n} \ [\ \ldots \\ & \ldots \ \max_{i_c=-|i_b|}^{|i_b|} \ \max_{j_c=-|j_b|}^{|j_b|} \ \max_{\substack{k_c=-n \\ (\vec{a}_{\rm SS}\times\vec{b}_{\rm SS})\cdot\vec{c}_{\rm SS}=V_{\rm SS}}}^{n} \mathcal{O}(\vec{a}_{\rm SS}, \vec{b}_{\rm SS}, \vec{c}_{\rm SS}) \ ] \end{aligned} \tag{2}$$

The volume of the supercell can only be a multiple of primitive cell volume, $V_{\rm SS} = mV_{\rm P}$. For a given volume ratio, m, one needs to decide what optimization criteria, $\mathcal{O}$, to employ. There are two obvious choices.

(a) First one can maximize the distance to the nearest periodic image, $d_{\rm min}$. In the limit of large m, this will not lead to formation of cubic cells. Rather hexagonal cells with $|\vec{a}_{\rm SS}| = |\vec{b}_{\rm SS}| = |\vec{c}_{\rm SS}|$, $\alpha = \beta = 90^\circ$, and $\gamma = 120^\circ$ will be favored [1] . While this may be a valid criteria for some problems, for fcc systems, it means that the conventional cubic supercells would not be reproduced.

(b) Alternatively one can design compact cells by minimizing the radius of a sphere that is needed to enclose the supercell. For a given cell, this radius is given by the maximum distance that any cell corner is separated from the cell center,

$$R_{\rm max} = \max_{\substack{i\,=\,\{-1,\,+1\}\\ j\,=\,\{-1,\,+1\}\\ k\,=\,\{-1,\,+1\}}} \frac{1}{2} \left| i\vec{a}_{\rm SS} + j\vec{b}_{\rm SS} + k\vec{c}_{\rm SS} \right| \ . \tag{3}$$

This criteria allows us to pick cubic and nearly cubic cells. For the remainder of this article, we employ the following optimization strategy. We use (b) as our primary criteria. If the $R_{\rm max}$ values of two cells are identical, we select the cell with the larger minimum image distance, $d_{\rm min}$. In rare cases where both of those values are identical also, we prefer the cell where the angles deviate the least from 90° and where the cell vectors deviate the least from each other in length.

The minimum image distance is defined as,

$$d_{\rm min} = \lim_{n=1}^{\infty} \min_{\substack{(i,\,j,\,k)\,=\,-n\\ i^2\,+\,j^2\,+\,k^2\,>\,0}}^{n} \left| i\vec{a}_{\rm SS} + j\vec{b}_{\rm SS} + k\vec{c}_{\rm SS} \right| \ , \tag{4}$$

but one needs a more efficient method for its determination that is applicable to arbitrary cell shapes. We use the following approach where the lattice vectors are re-assigned to point to closer images. We start with the assignment, $\vec{a}'_{\rm SS} = \vec{a}_{\rm SS}$, $\vec{b}'_{\rm SS} = \vec{b}_{\rm SS}$, and $\vec{c}'_{\rm SS} = \vec{c}_{\rm SS}$ and order the vectors by magnitude such that, $|\vec{a}'_{\rm SS}| \le |\vec{b}'_{\rm SS}| \le |\vec{c}'_{\rm SS}|$. Then we successively derive new vectors that point to closer and closer images using the following re-assignments,

$$\vec{b}'_{\rm SS} \ \rightarrow \ \vec{b}'_{\rm SS} - \vec{a}'_{\rm SS}\,{\rm round}\,[\,\vec{b}'_{\rm SS}\cdot\vec{a}'_{\rm SS}\,/\,\vec{a}'^2_{\rm SS}\,]\ , \tag{5}$$

$$\vec{c}'_{\rm SS} \ \rightarrow \ \vec{c}'_{\rm SS} - \vec{a}'_{\rm SS}\,{\rm round}\,[\,\vec{c}'_{\rm SS}\cdot\vec{a}'_{\rm SS}\,/\,\vec{a}'^2_{\rm SS}\,]\ , \tag{6}$$

$$\vec{c}'_{\rm SS} \ \rightarrow \ \vec{c}'_{\rm SS} - \vec{b}'_{\rm SS}\,{\rm round}\,[\,\vec{c}'_{\rm SS}\cdot\vec{b}'_{\rm SS}\,/\,\vec{b}'^2_{\rm SS}\,]\ . \tag{7}$$

We keep re-assigning and re-ordering these vectors until no more changes occur. Then we can derive $d_{\rm min}$ from $\vec{a}'_{\rm SS}$, $\vec{b}'_{\rm SS}$, and $\vec{c}'_{\rm SS}$ by setting $n = 1$ in Eq. (4).

3. Discussion of Cell Design

In Fig. 1, we plotted $R_{\rm max}$ and $d_{\rm min}$ for the supercells that we constructed by starting from the primitive cell of fcc lattice. For every cell size $V_{\rm SS}/V_{\rm P}$, we identified the most compact cell according to the optimization criteria that we derived in the previous section. The goal was to construct cells with an $R_{\rm max}$ that is as close as possible to the ideal value

[1] We derived this result using a simulated annealing technique that optimized minimum image distance by varying all cell parameters at constant volume.

N	$\frac{V_{\mathrm{SS}}}{V_{\mathrm{P}}}$	$\frac{R_{\mathrm{max}}}{a}$	$\frac{d_{\mathrm{min}}}{a}$	i_a	j_a	k_a	i_b	j_b	k_b	i_c	j_c	k_c	$\frac{\lvert a_{\mathrm{SS}}\rvert}{a}$	$\frac{\lvert b_{\mathrm{SS}}\rvert}{a}$	$\frac{\lvert c_{\mathrm{SS}}\rvert}{a}$	$\alpha(^\circ)$	$\beta(^\circ)$	$\gamma(^\circ)$
3	1	0.791	0.707	1	0	0	1	-1	0	0	0	-1	0.707	0.707	0.707	90	120	60
12	4†	0.866	1.000	1	1	-1	1	-1	1	1	-1	-1	1.000	1.000	1.000	90	90	90
21	7	1.118	1.225	1	1	0	-1	2	-1	-1	0	2	1.225	1.225	1.225	100	80	80
39	13	1.500	1.581	2	1	-1	2	-1	-2	-1	1	-2	1.581	1.581	1.581	72	107	72
69	23	1.768	1.732	3	-1	0	-1	3	-1	-1	0	3	1.871	1.732	1.871	90	86	108
78	26	1.732	1.871	2	1	0	-2	3	-1	-2	0	3	1.871	1.871	1.871	86	94	94
96	32†	1.732	2.000	2	2	-2	2	-2	2	2	-2	-2	2.000	2.000	2.000	90	90	90
114	38	1.871	2.121	2	2	-1	-2	3	-2	-2	1	3	2.121	2.121	2.121	93	87	87
150	50	2.121	2.345	2	1	1	-2	4	-1	-2	-1	4	2.345	2.345	2.345	98	82	82
210	70	2.424	2.549	3	2	-2	-2	4	-3	-2	2	3	2.549	2.739	2.549	90	88	80
276	92	2.549	2.739	4	1	-2	-3	4	2	-1	3	-4	2.739	3.082	2.739	88	88	95
288	96	2.500	2.828	4	-4	0	-3	-3	3	0	0	-4	2.828	3.000	2.828	90	90	90
300	100	2.693	2.916	4	1	-1	-2	5	-1	-1	-1	5	2.916	2.916	3.000	93	87	80
324	108†	2.598	3.000	3	3	-3	3	-3	3	3	-3	-3	3.000	3.000	3.000	90	90	90

Table 1: Supercells of the fcc structure with 3 atoms per primitive cell, which is needed to calculation of dense, superionic water. N specifies the number of atoms per cell. $V_{\mathrm{SS}}/V_{\mathrm{P}}$ is the volume ratio of the supercell and the primitive cell. R_{max} and d_{min} are the cell radii and minimum image distances according to Eqs. 3 and 4. The supercells are defined in terms of the integers i, j, and k (Eq. 2), lattice parameters and angles. All dimensional parameters have been normalized with respect to the lattice parameter a. Cubic cells with $V_{\mathrm{SS}}/V_{\mathrm{P}} = 4n^3$ are marked by a †.

N	$\frac{V_{\mathrm{SS}}}{V_{\mathrm{P}}}$	$\frac{R_{\mathrm{max}}}{a}$	$\frac{d_{\mathrm{min}}}{a}$	i_a	j_a	k_a	i_b	j_b	k_b	i_c	j_c	k_c	$\frac{\lvert a_{\mathrm{SS}}\rvert}{a}$	$\frac{\lvert b_{\mathrm{SS}}\rvert}{a}$	$\frac{\lvert c_{\mathrm{SS}}\rvert}{a}$	$\alpha(^\circ)$	$\beta(^\circ)$	$\gamma(^\circ)$
12	1†	0.866	1.000	1	0	0	0	1	0	0	0	-1	1.000	1.000	1.000	90	90	90
36	3	1.500	1.414	1	0	1	1	1	0	1	-1	-1	1.414	1.414	1.732	90	90	60
84	7	2.062	1.732	2	0	1	1	2	0	1	-1	-1	2.236	2.236	1.732	105	75	66
96	8†	1.732	2.000	2	0	0	0	2	0	0	0	-2	2.000	2.000	2.000	90	90	90
156	13	2.291	2.236	2	1	1	1	-2	-1	0	-1	2	2.449	2.449	2.236	90	79	100
168	14	2.236	2.449	2	1	1	1	-2	-1	-1	-1	2	2.449	2.449	2.449	100	100	100
288	24	2.500	2.828	3	0	0	0	2	2	0	2	-2	3.000	2.828	2.828	90	90	90
324	27†	2.598	3.000	3	0	0	0	3	0	0	0	-3	3.000	3.000	3.000	90	90	90
396	33	2.872	3.162	3	1	0	1	-3	-1	0	-1	3	3.162	3.317	3.162	90	96	90
456	38	3.202	3.317	3	1	1	2	-3	0	-1	-1	3	3.317	3.606	3.317	85	95	75
624	52	3.240	3.606	4	0	0	0	3	2	0	2	-3	4.000	3.606	3.606	90	90	90
672	56	3.500	3.742	3	2	1	2	-3	-2	-1	2	-3	3.742	4.123	3.742	97	98	97
768	64†	3.464	4.000	4	0	0	0	4	0	0	0	-4	4.000	4.000	4.000	90	90	90
876	73	3.905	4.123	4	1	1	1	-4	-1	0	-1	4	4.243	4.243	4.123	90	80	93
912	76	3.742	4.243	4	1	1	1	-4	-1	-1	-1	4	4.243	4.243	4.243	93	93	93
1116	93	4.062	4.359	3	3	1	3	-3	-2	-1	2	-4	4.359	4.690	4.583	93	93	96
1200	100	4.031	4.472	5	0	0	0	4	2	0	2	-4	5.000	4.472	4.472	90	90	90

Table 2: Supercells of the simple cubic pyrite structure with $N = 12$ atoms per primitive cell. All parameters are given in the format of Tab. 1. Cubic cells with $V_{\mathrm{SS}}/V_{\mathrm{P}} = n^3$ are marked by a †.

N	$\frac{V_{\mathrm{SS}}}{V_{\mathrm{P}}}$	$\frac{R_{\mathrm{max}}}{a}$	$\frac{d_{\mathrm{min}}}{a}$	i_a	j_a	k_a	i_b	j_b	k_b	i_c	j_c	k_c	$\frac{\lvert a_{\mathrm{SS}}\rvert}{a}$	$\frac{\lvert b_{\mathrm{SS}}\rvert}{a}$	$\frac{\lvert c_{\mathrm{SS}}\rvert}{a}$	$\alpha(^\circ)$	$\beta(^\circ)$	$\gamma(^\circ)$
1	1	0.829	0.866	1	0	0	1	-1	-1	0	-1	0	0.866	0.866	0.866	70	109	70
2	2†	0.866	1.000	1	0	-1	1	-1	0	0	-1	-1	1.000	1.000	1.000	90	90	90
6	6	1.479	1.414	2	-1	-2	-1	2	1	-1	0	-1	1.658	1.414	1.414	90	90	115
9	9	1.479	1.658	2	0	-1	1	-2	-2	-1	1	-1	1.658	1.658	1.658	85	95	85
16	16†	1.732	2.000	2	0	-2	2	-2	0	0	-2	-2	2.000	2.000	2.000	90	90	90
21	21	2.062	2.179	3	-1	-2	-1	3	1	-1	0	-2	2.236	2.179	2.179	87	96	96
25	25	2.278	2.236	3	-1	-3	-2	3	1	-1	-1	-2	2.598	2.236	2.236	90	85	105
28	28	2.236	2.449	3	0	-1	2	-3	-3	-1	1	-2	2.449	2.449	2.449	80	100	80
35	35	2.278	2.598	3	0	-2	-2	3	0	0	-2	-3	2.598	2.598	2.598	88	92	88
48	48	2.500	2.828	3	0	-3	2	-4	-2	-2	0	-2	3.000	2.828	2.828	90	90	90
53	53	2.861	2.958	3	1	-1	3	-3	-4	-2	3	-1	2.958	3.000	3.162	96	84	74
54	54†	2.598	3.000	3	0	-3	3	-3	0	0	-3	-3	3.000	3.000	3.000	90	90	90
65	65	3.031	3.279	4	0	-1	3	-4	-4	-1	1	-3	3.279	3.279	3.279	78	102	78
84	84	3.112	3.317	4	0	-2	2	-4	-4	-2	3	-2	3.317	3.317	3.841	92	88	85
91	91	3.112	3.571	4	0	-3	-3	4	0	0	-3	-4	3.571	3.571	3.571	89	91	89
103	103	3.345	3.606	5	-1	-2	-2	5	3	0	-1	4	3.742	3.606	3.841	92	94	94
107	107	3.419	3.742	5	-1	-2	2	-5	-4	-1	2	-3	3.742	3.841	3.742	90	94	86
112	112	3.419	3.841	5	-1	-1	-1	5	1	-1	1	5	3.841	3.841	3.841	95	85	85
128	128†	3.464	4.000	4	0	-4	4	-4	0	0	-4	-4	4.000	4.000	4.000	90	90	90

Table 3: Supercells of the bcc lattice with one atom per primitive cell. All parameters are given in the format of Tab. 1. Cubic cells with $V_{\mathrm{SS}}/V_{\mathrm{P}} = 2n^3$ are marked by a †.

N	$\frac{V_{\rm SS}}{V_{\rm P}}$	$\frac{R_{\rm max}}{a}$	$\frac{d_{\rm min}}{a}$	i_a	j_a	k_a	i_b	j_b	k_b	i_c	j_c	k_c	$\frac{\lvert a_{\rm SS}\rvert}{a}$	$\frac{\lvert b_{\rm SS}\rvert}{a}$	$\frac{\lvert c_{\rm SS}\rvert}{a}$	$\alpha(^\circ)$	$\beta(^\circ)$	$\gamma(^\circ)$
2	1	0.668	0.561	1	0	0	1	1	0	0	0	1	0.561	0.561	0.916	90	90	60
6	3	0.958	0.916	2	1	0	1	-1	0	0	0	-1	0.972	0.972	0.916	90	90	60
12	6	1.075	0.972	2	2	1	1	1	-1	-1	1	0	1.449	1.075	0.972	90	90	98
16	8	1.122	1.122	2	0	0	1	2	1	1	2	-1	1.122	1.336	1.336	87	90	90
22	11	1.365	1.336	3	1	0	1	2	1	0	-2	1	1.485	1.336	1.449	93	82	76
28	14	1.476	1.449	2	-1	1	-2	-2	1	0	-2	-1	1.745	1.449	1.449	96	80	78
32	16	1.449	1.485	3	1	0	-1	-3	0	0	0	-2	1.485	1.485	1.833	90	90	98
42	21	1.554	1.745	3	1	1	2	3	-1	-1	2	1	1.745	1.745	1.745	85	95	85
54	27	1.745	1.917	3	0	1	3	3	-1	0	-3	-1	1.917	1.917	1.917	99	81	81
74	37	1.896	2.023	4	1	0	-1	-4	-1	-1	-2	2	2.023	2.221	2.075	87	96	88
78	39	1.978	2.075	4	2	1	1	-3	-1	-1	-2	2	2.149	2.221	2.075	93	80	89
84	42	2.017	2.149	3	-1	1	-3	-4	1	0	-2	-2	2.221	2.221	2.149	91	91	82
106	53	2.168	2.221	4	0	1	3	4	-1	0	-3	-2	2.425	2.221	2.489	97	88	85
124	62	2.297	2.359	5	2	0	-1	-4	2	-1	-3	-2	2.446	2.730	2.359	93	98	95
130	65	2.342	2.425	4	0	1	3	4	-2	0	-3	-2	2.425	2.730	2.489	82	88	94
138	69	2.297	2.446	5	1	0	-2	-5	0	0	0	-3	2.572	2.446	2.749	90	90	94
152	76	2.398	2.612	4	2	2	3	4	-2	-2	3	1	2.672	2.730	2.612	90	92	94
160	80	2.398	2.672	5	0	0	2	4	2	2	4	-2	2.806	2.672	2.672	87	90	90
176	88	2.441	2.730	5	0	1	3	4	-2	-1	-4	-2	2.952	2.730	2.730	91	91	91
180	90	2.446	2.749	6	3	0	0	-5	0	0	0	-3	2.916	2.806	2.749	90	90	90
200	100	2.567	2.806	5	0	0	3	6	1	1	2	-3	2.806	3.057	2.916	88	90	90

Table 4: Supercells of hexagonal close packed lattice with the ideal ratio, $c/a = \sqrt{8/3}$. All parameters are given in the format of Tab. 1.

of cube, $V_{\rm SS}^{1/3}\sqrt{3}/2$. For cubic cells with $V_{\rm SS}/V_{\rm P} = 4n^3$, this value is recovered. For all other cells, $R_{\rm max}$ is found to reasonably close to the ideal value. The deviations are typically no larger than $0.25\,a$, where a is the size of the cubic.

The lower panel Fig. 1 shows the minimum image distances for every cell. For a given cell size, this value should be as large as possible in order to minimize the correlation effects between particles during molecular dynamics simulations. One notices that for some cells, the $d_{\rm min}$ falls above the curve for a cubic cell given by $d_{\rm min}^{\rm cubic} = V_{\rm SS}^{1/3}$. This is because hexagonal cells, rather than cubic ones, have the largest minimum image distances for given volume.

Furthermore one notices that $d_{\rm min}$ does not monotonously increase with volume. One would have expected that a larger cell size automatically leads to an increase in the minimum image distance. However, the constructed cells differ in shape and in many cases, the minimum image distance of a larger cell is smaller or equal to that of a well-selected smaller one. So it is not obvious why one should invest the computer time into simulating with a larger cell if it does not also lead to an increase in the minimum image distance over all possible smaller cells. For this reason, we selected a subset of cells where an increase in size also leads to a new record in the minimum image distance compared to all smaller cells. We marked the cells in this subset with circles and squares in Fig. 1 and reported their parameters in Tab. 1. The ideal cubic cells are included in the subset. From now on we refer to this subset as set of *compact* cells. All DFT-MD simulations, to be discussed in this article, were performed for such compact supercells. Tables 2, 3, and 4 list the parameters for the compact supercells for simple cubic, bcc, and hexagonal close packed lattices, respectively.

The angles and supercell vector lengths in Tab. 1 show that it becomes easier to construct nearly cubic supercells with increasing cell size. For large supercells there are simply more possibilities to combine the primitive cells to construct supercells with specific size. In the limit of infinite supercells size, one expects the deviations from a cubic shape to disappear completely. Already for $V_{\rm SS}/V_{\rm P} \geq 13$, one finds that all cell angles deviate from 90° by 10.5° or less. All vector lengths deviate by less then 8.5% from the corresponding value of a cubic cell.

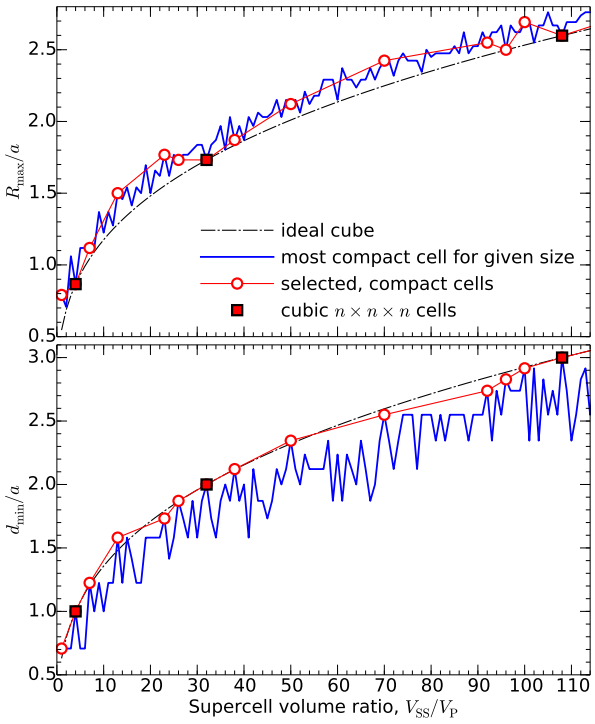

Figure 1: (Color online) Radius, $R_{\max}$, (Eq. 3) and minimum image distance, $d_{\min}$, (Eq. 4) of supercells that were constructed from the primitive cell of fcc lattice with lattice parameter a. The solid, blue lines correspond to cells with smallest $R_{\max}$ for a given cell volume. The open circles correspond to a subset of selected, compact cells that have a larger minimum image distance than all smaller cells. The squares denote cubic supercells with $V_{SS} = 4n^3 V_P$ where n is an integer. The dash-dotted line shows $R_{\max}$ and $d_{\min}$ for a cubic cell of arbitrary, non-integer values of n.

4. Accommodation of Two Crystal Structures

Our optimization scheme in Eq. 2 is general and can be combined with other design criteria, $\mathcal{O}(\vec{a}_{SS}, \vec{b}_{SS}, \vec{c}_{SS})$, for specific applications. We will give one more example in this section where we design supercells that can accommodate two different crystal structures. We will construct supercells that are commensurate with, e.g., an fcc and an hcp lattice, which becomes of interest for crystallization calculations where one wants to eliminate, or at least minimize, the bias from a particular supercell choice. This is of interest for the simulation of materials that show an hcp-fcc transition in their pressure-temperature phase diagrams, such as gold [57], iron at 30 GPa and elevated temperatures [58] as well as at 700 GPa and low temperature [59], iron-nickel alloys at conditions of the Earth's core [60] and many others.

The task of finding a supercell that accommodates two crystal structures shares some similarities with constructing approximate, commensurate cells for incommensurate structures [28, 29] where one needs to capture the periodicities among the host and

	N	$\frac{\delta}{a}$	i_a	j_a	k_a	i_b	j_b	k_b	i_c	j_c	k_c	$\frac{\lvert a_{SS}\rvert}{a}$	$\frac{\lvert b_{SS}\rvert}{a}$	$\frac{\lvert c_{SS}\rvert}{a}$	$\alpha(^\circ)$	$\beta(^\circ)$	$\gamma(^\circ)$
hcp:	156	0	5	7	0	-3	1	0	0	0	3	6.245	3.606	4.899	90	90	90
fcc:			5	-7	2	-3	-1	4	2	2	2	6.245	3.606	4.899	90	90	90
hcp:	480	0	6	6	3	-4	4	0	-4	-4	3	7.746	6.928	6.325	90	90	90
fcc:			-6	8	-4	0	-4	-4	6	2	-6	7.746	6.928	6.325	90	90	90
bcc:	160	0.045	5	0	5	4	4	0	0	4	4	5.000	4.000	4.000	90	90	90
fcc:			4	4	-4	2	-2	-4	-4	4	-2	5.040	3.984	3.984	90	90	90
bcc:	847	0.027	7	-4	2	-6	-8	-7	4	3	-7	7.921	6.225	8.602	89	88	87
fcc:			-7	-3	10	-6	2	-3	4	-11	0	7.918	6.236	8.592	89	88	87

Table 5: Supercells that can accommodate hcp and fcc crystals as well as bcc and fcc crystals. N specifies the number atoms per cell. The mismatch parameter, δ, and the supercell vectors are given in units of lattice parameter $a_{\rm bcc}$ and $a_{\rm hcp}$, respectively.

the guest atoms [61]. However, there is one important difference. In our case, there is no need for both structures to be aligned in the supercell. In fact, when we minimize the mismatch between hcp and fcc supercell vectors, we allow for an arbitrary rotation by the Euler angles, ϕ,θ, and ψ. We introduce the rotation matrix, $\mathcal{R}_{\phi,\theta,\psi}$, and define the mismatch parameter,

$$\delta_{\rm fcc-hcp} = \min_{\phi,\theta,\psi} \left[(\vec{a}_{\rm SS}^{\rm fcc} - \mathcal{R}_{\phi,\theta,\psi}\, \vec{a}_{\rm SS}^{\rm hcp})^2 + (\vec{b}_{\rm SS}^{\rm fcc} - \mathcal{R}_{\phi,\theta,\psi}\, \vec{b}_{\rm SS}^{\rm hcp})^2 + (\vec{c}_{\rm SS}^{\rm fcc} - \mathcal{R}_{\phi,\theta,\psi}\, \vec{c}_{\rm SS}^{\rm hcp})^2 \right]^{1/2} , \tag{8}$$

that measures the deviation between the both sets of lattice vectors. We minimize δ by first determining the 100 most compact hcp supercells for a given size. For each hcp supercell, a pick a random rotation matrix, and identify the closest set of fcc lattice vectors. We use the BGFS algorithm [62] to optimize the Euler angles in order to converge to the closest local minimum of δ. This procedure is repeated many times in an attempt to find the global minimum of δ. The goal of this optimization is to construct supercells that can accommodate fcc and hcp lattices.

Figure 2 and Table 5 report the best supercells that we constructed. We able to obtain two compact supercells with respectively 156 and 480 atoms that accommodate and hcp and fcc lattices perfectly. Many other supercells with a small mismatch parameter of $\delta < 0.07\, a_{\rm hcp}$ have been identified as well.

We also constructed supercells that can accommodated a bcc as well as an fcc crystal structure, which would be of interest for the simulation of sodium [63], lithium [64], xenon [65], and Yukawa systems [66]. One could expect that accommodating an bcc and an fcc structures in one supercell to be straightforward because both are cubic structures. However, one would want to keep the particle density the same, which implies there bcc and fcc lattice parameters differ by a factor of $2^{1/3}$. Since this is an irrational ratio, we cannot expect to find a supercell that accommodates both crystals perfectly. Still our best cells in Tab. 5 with $N = 160$ and 847 atoms have a small mismatch, δ, of only 0.0455 and 0.0270 $a_{\rm bcc}$, which means the lattice vectors differ by less than 0.8% and 0.2% respectively. The impact of this deviation may be reduced further by setting the lattice vectors in the simulation to the average of the bcc and fcc supercell vectors so that both structures are affected equally by the constraints of the supercell.

5. Results from Ab Initio Simulations

In this section, we compare the internal energy and pressure that we obtained with DFT-MD simulations in compact supercells of various sizes. To cover a range of appli-

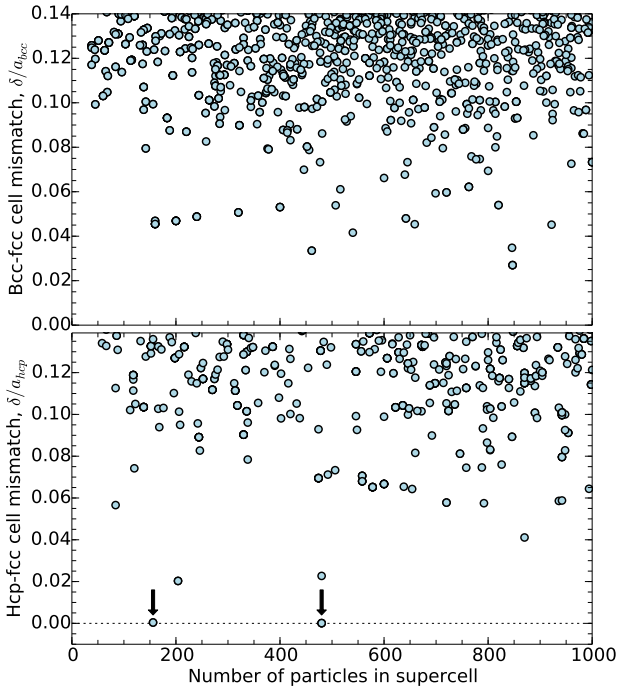

Figure 2: (Color online) Mismatch parameter, δ, (Eq. 8) between bcc and hcp lattices (upper panel) and fcc and hcp lattices (lower panel) for supercells with different numbers of particles. δ is plotted in units of lattice parameter $a_{\rm bcc}$ and $a_{\rm hcp}$, respectively. The arrows in the lower panel mark cells with 156 and 480 atoms, respectively, that can perfectly accommodate an hcp and an fcc lattice.

cations, we selected three representative systems with very different character. First we presents results of diamond, a hard, monatomic, covalently bonded solid. As an example for an ionic material, we discuss simulations of SiO_2 silica in the cubic pyrite structure. Finally we compare results for superionic water where the oxygen atoms are arranged on a fcc lattice. Superionic behavior [67] may occur in materials like α-AgI that are composed of ions with very different radii. The large ions, in this case I^-, remain locked in place and vibrate around lattice site like atoms in a solid while the smaller ions, Ag^+, move throughout the lattice like a fluid. This behavior has been predicted theoretically to occur in water at megabar pressures [68]. Recent simulations predicted a phase change to an fcc oxygen sub-lattice [40].

All DFT-MD simulations were performed with the VASP code [69]. We used pseudopotentials of the projector-augmented wave type [70], the exchange-correlation functional of Perdew, Burke and Ernzerhof [71], and a cutoff energy of 900 eV for the plane wave expansion of the wavefunctions. The Brillioun zone was sampled with the zone-average Balderesci point [72] as well as with $2 \times 2 \times 2$ and $4 \times 4 \times 4$ Monkhorst-Pack k-point grids [73]. The occupation of electronic states are taken to be a Fermi-Dirac distribution set at the temperature of the ions [74]. The simulation time ranged between

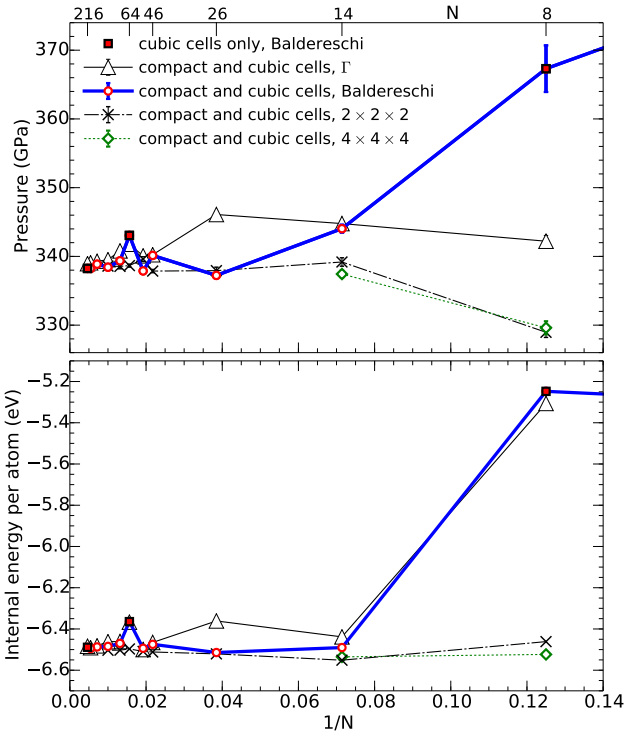

Figure 3: (Color online) Pressure and internal energy of diamond derived from DFT-MD simulations at 5000 K and 5.02 g cm^{-3} using compact supercells with different numbers of atoms, N and k-point grids for the Brillioun zone sampling. Error bars are shown unless they are smaller than the size of the symbols. For zone-average Baldaresci k-point curve, we used squares to mark cases where the constructed, compact cells coincided with the standard, cubic supercells with $N = 8n^3$.

2.0 and 10.0 ps. An MD time step of 0.20, 0.75, and 0.80 fs was used for ice, diamond, and SiO_2, respectively.

Finite size effects in DFT-MD simulations with periodic boundary conditions do not only arise from a finite number of ions and but also from an incomplete sampling of the Brillioun zone. One cannot completely separate one effect from the other because of k-point folding. When a supercell is constructed using a fixed set of k-points, this already implies a more accurate Brillioun zone sampling compared to the primitive cell. This is the reason why one typically uses a very small number of k-points in DFT-MD simulations and rather invests the available CPU time into simulating more atoms. Earlier simulations of dense carbon used the Γ point but more recent work employed the Baldaresci point [11]. Figure 3 shows pressure and internal energy derived from simulations of various cell sizes. A typical supercell with $64{=}8{\times}2^3$ atoms [11] yielded a pressure of 344 GPa. Relying on cubic supercells alone, would make it very challenging to determine the magnitude of the remaining finite size error (-1.4% in pressure) and correct for it efficiently. One could compare with the results from simulations in a tiny cell

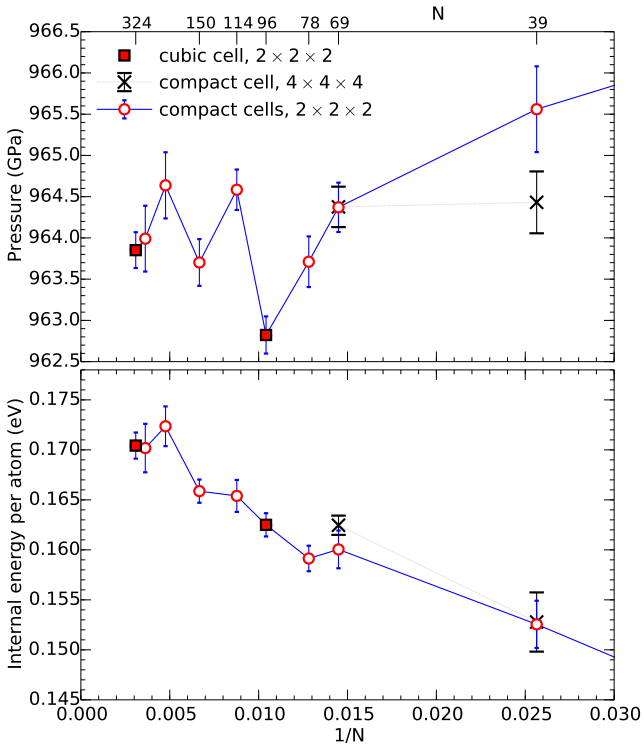

Figure 4: (Color online) Pressure and internal energy of fcc superionic ice from DFT-MD simulations at 4000 K and 6.00 g cm^{-3} using compact supercells with different numbers of atoms, N, and k-point grids for the Brillioun zone sampling.

with 8 atoms, the only available cubic cell that is smaller, and then linear extrapolation as function of $1/N$. One would not know, however, how reliable such an extrapolation would be unless one obtains results the next larger cubic cell with $216{=}8{\times}3^3$ atoms. As Fig. 3 shows, we were able to perform such large simulations and confirm that the extrapolations for the pressure and energy are reasonably accurate but this test required a disproportionate amount of computer time. For more complex minerals that have unit cells with more atoms, such large supercell calculation may not be feasible.

Fig. 3 also shows simulation results based on our compact supercells that we constructed by starting from a 2 atom primitive cell of the fcc lattice. The supercell parameters are given in Tab. 1. Both pressures and internal energies from simulations with 76, 100, 140, and 184 atoms are in very good agreement with 216 atom results. This highlights the quality of the compact supercells that we constructed. Simulations with smaller cells are significantly faster. This also makes easier to determine how long one needs to run simulation to reach a certain accuracy.

The results from simulations with the Baldereschi point in Fig. 3 show an overall trend for pressure and energy to decrease with system size. This is partially due to insufficient sampling of the Brillioun zone. Results from simulation of with $2 \times 2 \times 2$ and $4 \times 4 \times 4$

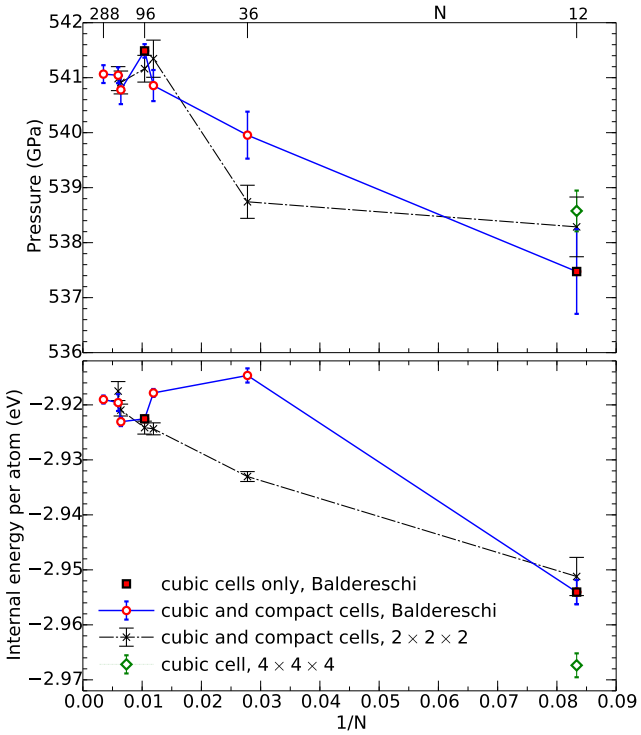

Figure 5: (Color online) Pressure and internal energy of silica, SiO_2, in the cubic pyrite structure from DFT-MD simulations at 5000 K and 7.56 g cm^{-3} using compact supercells with different numbers of atoms, N, and k-point grids.

k-point grids converge much faster with system size and pressure and energy tend to increase with system size.

We select superionic water as the next test case for the application of our compact supercells. In each case, we started from a perfect fcc oxygen sub-lattice and then gradually increased the temperature in the DFT-MD simulations until the system reached a temperature of 4000 K where the system is superionic. In Fig. 4, we show results for seven cell sizes in addition to the two cubic supercells with 32=4×2^3 and 108=4×3^3 H_2O molecules used in Ref. [40]. $2 \times 2 \times 2$ k-point grids was employed in most calculations but two tests with $4 \times 4 \times 4$ points were performed.

A linear trend in the energy per atoms, N, appears as a function of $1/N$. Our compact cells follow this trend in the same way as the two cubic cells. One finds the energy value of 0.1625 eV/atom from simulations of 32 molecules is not yet converged but that an extrapolated value of 0.173 eV/atom is more realistic. The pressure appears to converge to a value of approximately 964.3 GPa. Simulations with a cubic supercell containing 32 molecules appear to yield a pressure that is slightly too low. The simulations with $4 \times 4 \times 4$ k-points are broadly consistent with the $2 \times 2 \times 2$ results, only for simulations with 13 molecules there is a deviation in the pressure.

In Tab. 3, we list 6 intermediate cell sizes that could have been used to study finite size effects in simulations of bcc solids in addition to the cubic cells with $54=2\times3^3$ and $128=2\times4^3$ molecules used in Ref. [41].

Finally, we come to the discussion of the finite size effects in DFT-MD simulations of silicate in the pyrite structure. Since the primitive cubic cell already has 4 SiO_2 molecules, a finite size extrapolations on cubic cells alone would be very challenging. Using the supercell in Tab. 2, we performed simulations with up to 288 atoms. Results in Fig. 5 show that finite size error in cubic simulations 96 atoms with the Baldereschi point is already very small. The pressure appears to be overestimated by only 0.4 GPa. The correction to the internal energy is also very small, only on the order of 4 meV per atom.

6. Conclusions

We designed and tested a general algorithm for constructing compact supercells for first-principles simulations of solids. Results for common structures such as sc, bcc, fcc, and hcp lattices were reported. Since we started from the primitive cell, we were able to construct compact supercells of intermediate sizes that cannot be obtained with simple replication of the conventional unit cell. This allowed us to perform a more detailed a finite size analysis of the DFT-MD simulations of diamond, SiO_2, and superionic water. We demonstrate that the compact supercells can be used the estimate finite size effects and in most cases, to extrapolate to thermodynamic limit with good precision. We anticipate this will make predictions from computer simulations more reliable for applications where very large simulation with 1000 atoms or more are still prohibitively expensive. In addition to the presented computation of thermodynamic properties, our algorithm can be used to construct supercells to study systems with defects, solid solutions, magnetic and superionic systems. While we tested our approach only in DFT-MD simulations, future applications will include quantum Monte Carlo calculations where it is even more difficult to study large systems routinely.

Acknowledgments

This research is supported by the U. S. Department of Energy, grants DE-SC0010517 and DE-SC0016248.

References

[1] M. E. Tuckermann, J. Phs. Cond. Matter 14 (2002) R1297.
[2] B. Kirchner, P. J. di Dio, J. Hutter (Eds.), Real-World Predictions from Ab Initio Molecular Dynamics Simulations, Vol. 307 of Topics in Current Chemistry, Springer Berlin, 2012, p. 109.
[3] T. Tsuchiya, J. Tsuchiya, K. Umemoto, R. M. . Wentzcovitch, Proc. Nat. Acad. Sci. 108 (2011) 1252.
[4] K. P. Driver, R. E. Cohen, Z. Wu, B. Militzer, P. L. Rios, M. D. Towler, R. J. Needs, J. W. Wilkins, Proc. Nat. Acad. Sci. 107 (2010) 9519.
[5] T. Tsuchiya, J. Tsuchiya, Proc. Nat. Acad. Sci. 108 (2011) 1252.
[6] M. Parrinello, Solid State Comm. 102 (1997) 107.
[7] M. Allen, D. Tildesley, Oxford University Press, New York, 1987.
[8] B. Militzer, Phys. Rev. B 79 (2009) 155105.
[9] A. A. Correa, S. A. Bonev, G. Galli, Proc. Nat. Acad. Sci. 103 (2006) 1204.

[10] D. Alfè, M. Pozzo, M. P. Desjarlais, Phys. Rev. B 85 (2012) 024102.
[11] L. X. Benedict, K. P. Driver, S. Hamel, B. Militzer, T. Qi, A. A. Correa, E. Schwegler, "A multiphase equation of state for carbon addressing high pressures and temperatures", submitted to Phys. Rev. B (2013), available on arXiv:1311.4577.
[12] S. Zhang, S. Cottaar, T. Liu, S. Stackhouse, B. Militzer, High-pressure, temperature elasticity of fe- and al-bearing mgsio3: implications for the earth's lower mantle, Earth and Planetary Science Letters 434 (2016) 264.
[13] S. Baroni, S. de Gironcoli, A. D. Corso, Rev. Mod. Phys. 73 (2001) 515.
[14] A. Togo, F. Oba, I. Tanaka, Phys. Rev. B 78 (2008) 134106.
[15] G. Stapper, M. Bernasconi, N. Nicoloso, M. Parrinello, Physical Review B 59 (2) (1999) 797–810. doi:10.1103/PhysRevB.59.797, [link].
URL http://link.aps.org/doi/10.1103/PhysRevB.59.797
[16] F. Tasnádi, M. Odén, I. a. Abrikosov, Physical Review B 85 (14) (2012) 144112. doi:10.1103/PhysRevB.85.144112, [link].
URL http://link.aps.org/doi/10.1103/PhysRevB.85.144112
[17] J. Liu, D. Vanderbilt, Physical Review B 88 (22) (2013) 224202. doi:10.1103/PhysRevB.88.224202, [link].
URL http://link.aps.org/doi/10.1103/PhysRevB.88.224202
[18] a. Lindmaa, R. Lizárraga, E. Holmström, I. a. Abrikosov, B. Alling, Physical Review B 88 (5) (2013) 054414. doi:10.1103/PhysRevB.88.054414, [link].
URL http://link.aps.org/doi/10.1103/PhysRevB.88.054414
[19] M. Pesola, R. M. Nieminen, M. J. Puska, S. Po 58 (3) (1998) 1318–1325.
[20] L. Munro, D. Wales, Physical Review B 59 (6) (1999) 3969–3980. doi:10.1103/PhysRevB.59.3969, [link].
URL http://link.aps.org/doi/10.1103/PhysRevB.59.3969
[21] C. Domain, C. Becquart, J. Foct, Physical Review B 69 (14) (2004) 144112. doi:10.1103/PhysRevB.69.144112, [link].
URL http://link.aps.org/doi/10.1103/PhysRevB.69.144112
[22] A. J. Jackson, A. Walsh, Physical Review B 88 (16) (2013) 165201. doi:10.1103/PhysRevB.88.165201, [link].
URL http://link.aps.org/doi/10.1103/PhysRevB.88.165201
[23] C. Varvenne, F. Bruneval, M.-C. Marinica, E. Clouet, Physical Review B 88 (13) (2013) 134102. doi:10.1103/PhysRevB.88.134102, [link].
URL http://link.aps.org/doi/10.1103/PhysRevB.88.134102
[24] X. T. Trinh, K. Szász, T. Hornos, K. Kawahara, J. Suda, T. Kimoto, a. Gali, E. Janzén, N. T. Son, Physical Review B 88 (23) (2013) 235209. doi:10.1103/PhysRevB.88.235209, [link].
URL http://link.aps.org/doi/10.1103/PhysRevB.88.235209
[25] J. Pohl, K. Albe, Physical Review B 87 (24) (2013) 245203. doi:10.1103/PhysRevB.87.245203, [link].
URL http://link.aps.org/doi/10.1103/PhysRevB.87.245203
[26] F. Matusalem, M. Ribeiro, Jr., M. Marques, R. Pelá, L. Ferreira, L. Teles, Physical Review B 88 (22) (2013) 224102. doi:10.1103/PhysRevB.88.224102, [link].
URL http://link.aps.org/doi/10.1103/PhysRevB.88.224102
[27] H.-P. Komsa, A. Pasquarello, Physical Review Letters 110 (9) (2013) 095505. doi:10.1103/PhysRevLett.110.095505, [link].
URL http://link.aps.org/doi/10.1103/PhysRevLett.110.095505
[28] S. Lu, Q.-M. Hu, M. P. J. Punkkinen, B. Johansson, L. Vitos, Physical Review B 87 (22) (2013) 224104. doi:10.1103/PhysRevB.87.224104, [link].
URL http://link.aps.org/doi/10.1103/PhysRevB.87.224104
[29] H. Fujihisa, Y. Nakamoto, M. Sakata, K. Shimizu, T. Matsuoka, Y. Ohishi, H. Yamawaki, S. Takeya, Y. Gotoh, Physical Review Letters 110 (23) (2013) 235501. doi:10.1103/PhysRevLett.110.235501, [link].
URL http://link.aps.org/doi/10.1103/PhysRevLett.110.235501
[30] A. R. G. Rollmann, P. Entel, J. Hafner, Phys. Rev. B 69 (2004) 165107.
[31] R. O. Kuzian, I. V. Kondokova, A. M. Dare, V. V. Laguta, Phys. Rev. B 89 (2014) 024402.
[32] S. Grytsyuk, U. Schwingenschlögl, Phys. Rev. B 88 (2013) 165414.
[33] W. Ching, P. Rulis, Physical Review B 77 (12) (2008) 125116. doi:10.1103/PhysRevB.77.125116, [link].
URL http://link.aps.org/doi/10.1103/PhysRevB.77.125116

[34] D. Alfè, Phys. Rev. B 68 (2003) 064423.
[35] L. G.Wang, A. van de Walle, D. Alfe, Phys. Rev. B 84 (2011) 092102.
[36] S. Aryal, P. Rulis, W. Y. Ching, Phys. Rev. B 84 (2011) 184112.
[37] Y. G. Yu, R. J. Angel, N. L. Ross, G. V. Gibbs, Phys. Rev. B 87 (2013) 184112.
[38] K. P. Esler, R. E. Cohen, B. Militzer, J. Kim, R. J. Needs, M. Towler, Phys. Rev. Lett. 104 (2010) 185702.
[39] L. Shulenburger, T. R. Mattsson, Phys. Rev. B 88 (2013) 245117.
[40] H. F. Wilson, M. L. Wong, B. Militzer, Phys. Rev. Lett. 110 (2013) 151102.
[41] M. French, T. R. Mattsson, N. Nettelmann, R. Redmer, Phys. Rev. B 79 (2009) 054107.
[42] L. G. Ferreira, S.-H. Wei, A. Zunger, Int. J. Supercomput. Ap. 5 (1991) 34.
[43] A. van de Walle, G. Ceder, Automating first-principles phase diagram calculations, J. Phase Equilib. 23 (2002) 348.
[44] G. L. W. Hart, R. W. Forcade, Phys. Rev. B 77 (2008) 224115.
[45] B. Militzer, H. F. Wilson, Phys. Rev. Lett. 105 (2010) 195701.
[46] C. J. Pickard, M. Martinez-Canales, R. J. Needs, Phys. Rev. Lett. 110 (2013) 245701.
[47] A. R. Oganov, C. W. Glass, J. Chem. Phys. 124 (2006) 244704.
[48] C. J. Pickard, R. J. Needs, J. Phys. Condens. Matter 23 (2011) 053201.
[49] S. M. Woodley, R. Catlow, Nature Mat. 7 (2008) 937.
[50] Y. Ma, M. Eremets, R. O. A, Y. Xie, I. Trojan, S. Medvedev, A. O. Lyakhov, M. Valle, V. Prakapenka, Nature 458 (2008) 182.
[51] G. A. de Wijs, G. Kresse, M. J. Gillan, Phys. Rev. B 57 (1998) 8223.
[52] H. F. Wilson, B. Militzer, Phys. Rev. Lett. 104 (2010) 121101.
[53] H. F. Wilson, B. Militzer, Phys. Rev. Lett. 108 (2012) 111101.
[54] B. Militzer, Phys. Rev. B 87 (2013) 014202.
[55] S. M. Wahl, H. F. Wilson, B. Militzer, Astrophys. J. 773 (2013) 95.
[56] R. A. Evarestov, Quantum Chemistry of Solids, LCAO Treatment of Crystal and Nanostructures, Springer Heidelberg New York Dordrecht London, 2012.
[57] T. Ishikawa, K. Kato, M. Nomura, N. Suzuki, H. Nagara, K.Shimizu, Phys. Rev. B 88 (2013) 214110.
[58] S. K. Saxena, G. Shen, P. Lazor, Science 260 (1993) 1312.
[59] C. J. Pickard, R. J. Needs, J. Phys. Condens. Matter 21 (2009) 452205.
[60] A. S. Cote, L. Vocadlo, J. P. Brodhold, Earth Planet. Sci. Lett. 345 (2012) 185702.
[61] S. van Smaalen, Incommensurate Crystallography, University Press Scholarship Online, 2007. doi:10.1093/acprof:oso/9780198570820.001.0001.
[62] D. E. Jacobs, The State of the Art in Numerical Analysis, Academic Press, 1977.
[63] E. Gregoryanz, O. Degtyareva, M. Somayazulu, R. J. Hemley, H. k. Mao, Phys. Rev. Lett. 95 (2005) 185502.
[64] R. G. Munro, R. D. Mountain, Phys. Rev. B 28 (1983) 2261–2263. doi:10.1103/PhysRevB.28.2261, [link].
URL http://link.aps.org/doi/10.1103/PhysRevB.28.2261
[65] B. A. Belonoshko, O. LeBacq, R. Ahuja, B. Johansson, J. Chem. Phys. 117 (2002) 7233.
[66] R. T. Farouki, S. Hamguchi, J. Chem. Phys. 101 (1994) 9885.
[67] F. A. Karamov (Ed.), Superionic conductors, Cambridge International Science Pub., 2008.
[68] C. Cavazzoni, G. L. Chiarotti, S. Scandolo, E. Tosatti, M. Bernasconi, M. Parrinello, Nature 283 (1999) 44.
[69] G. Kresse and J. Hafner, Phys. Rev. B 47, 558 (1993); G. Kresse and J. Hafner, Phys. Rev. B 49, 14251 (1994); G. Kresse and J. Furthmüller, Comput. Mat. Sci. 6, 15 (1996); G. Kresse and J. Furthmüller, Phys. Rev. B 54, 11169 (1996).
[70] P. E. Blöchl, Phys. Rev. B 50 (1994) 17953.
[71] J. P. Perdew, K. Burke, M. Ernzerhof, Phys. Rev. Lett. 77 (1996) 3865.
[72] A. Balderesci, Phys. Rev. B 7 (1977) 5212.
[73] H. Monkhorst, J. Pack, Phys. Rev. B. 13 (1976) 5188.
[74] N. D. Mermin, Phys. Rev. 137 (1965) A1441.